Journal of Energy Storage 24 (2019) 100776

Contents lists available at ScienceDirect

Journal of Energy Storage

journal homepage: www.elsevier.com/locate/est

Synergistic effect of silver and adenine on boosting the supercapacitance performance of spongy graphene

Dalia M. El-Gendy[a,b], Nabil A. Abdel Ghany[b,*], Nageh K. Allam[a,*]

[a] Energy Materials Laboratory (EML), School of Sciences and Engineering, The American University in Cairo, New Cairo, 11835, Egypt
[b] Physical Chemistry Department, National Research Centre, Dokki, Giza, Egypt

ARTICLE INFO

Keywords:
Supercapacitor
Spongy
Graphene
Adenine
Energy density
Silver

ABSTRACT

A stable aqueous suspension of adenine-functionalized graphene/silver (FG/Ag) nanocomposites was prepared *via* a hydrothermal-assisted method. The fabricated FG/Ag nanocomposites were characterized by X-ray diffraction (XRD), FTIR, Raman spectroscopy, thermogravimetric analysis (TGA), UV–vis absorption spectroscopy and transmission electron microscopy (TEM). Field emission scanning electron microscopy (FESEM) imaging showed a uniform distribution of Ag nanoparticles on the FG surface, which increased the thermal stability of the material as confirmed via the thermogravimetric analysis (TGA). Upon their use as supercapacitor electrodes, the fabricated nanocomposites containing 20 wt% silver nitrate revealed a remarkable specific capacitance of 567/g at scan rate of 1 mV/s and excellent cycling retention of 100.5% after 1000 cycles at 200 mV/s with high energy density of 82.9Wh kg^{-1} in a three-electrode system and 37.03 Wh kg^{-1} when assembled in a symmetric device at 1 A/g, which are higher than those reported in literature for graphene-based materials. The superior electrochemical performance is ascribed to the synergistic effect of adenine functionalization and Ag doping.

1. Introduction

Electrochemical supercapacitors have attracted much attention in latest years owing to their high power density, reversibility, long cycle life, and environmentally-friendly nature [1]. According to their charge storage mechanism, they can be classified into two basic types; electric double-layer capacitors (EDLCs) and pseudocapacitors. While the EDLCs store energy physically by adsorption of charge accumulation at the electrode/electrolyte interface [2], the battery type, or pseudocapacitors, store energy chemically by fast and reversible Faradic reactions at the electrode materials [3]. The pseudocapacitive materials such as metal oxides [4] and conducting polymers [5] can attain relatively higher capacitance than EDLCs but are limited the by poor cyclability because of the degradation of the electrode structure during the redox process [6]. Therefore, carbonaceous materials are combined with either metal oxides or polymers to overcome the stability problem [7]. In this regard, many carbon-based materials are being investigated, such as carbon nanotubes, activated carbons (AC), and graphite. Graphene oxide and graphene are advantageous due to their availability, ease of preparation, and good stability [8]. Specifically, graphene has attracted much attention as an effective supercapacitor electrode material owing to its novel properties, including excellent electrical and mechanical properties, chemical stability, high specific surface area and the utility for large-scale fabrication of chemically modified graphene (CMGs) [9–13]. However, graphene suffers from the agglomeration and restacking of its nanosheets, rendering the material less effective. In this regard, graphene can be doped with foreign elements, such as N, B and S, to prevent the agglomeration and restacking [1,14–16]. On the other hand, graphene can be mixed with metal and metal oxide nanoparticles (NPs) to form NPs/graphene nanocomposites with catalytic activities [17–19]. For example, decoration of graphene with silver NPs was shown to efficiently prevent the aggregation and restacking of graphene nanosheets [20,21].

Herein, an environmentally friendly preparation method (Fig. 1) is developed to fabricate adenine-functionalized spongy graphene that is decorated with Ag NPs (FG/Ag). The FG/Ag sheets were obtained by using adenine as an N-dopant followed by the deposition of Ag NPs hydrothermally. The fabricated FG/Ag nanocomposites have been evaluated as supercapacitor electrode materials, showing exceptional performance. The morphology, structure and electrochemical properties of the as-prepared FG/Ag were studied in detail to explain the observed high performance.

* Corresponding authors.
E-mail addresses: na_manakhly@yahoo.co.uk (N.A. Abdel Ghany), nageh.allam@aucegypt.edu (N.K. Allam).

https://doi.org/10.1016/j.est.2019.100776
Received 9 March 2019; Received in revised form 21 April 2019; Accepted 12 May 2019

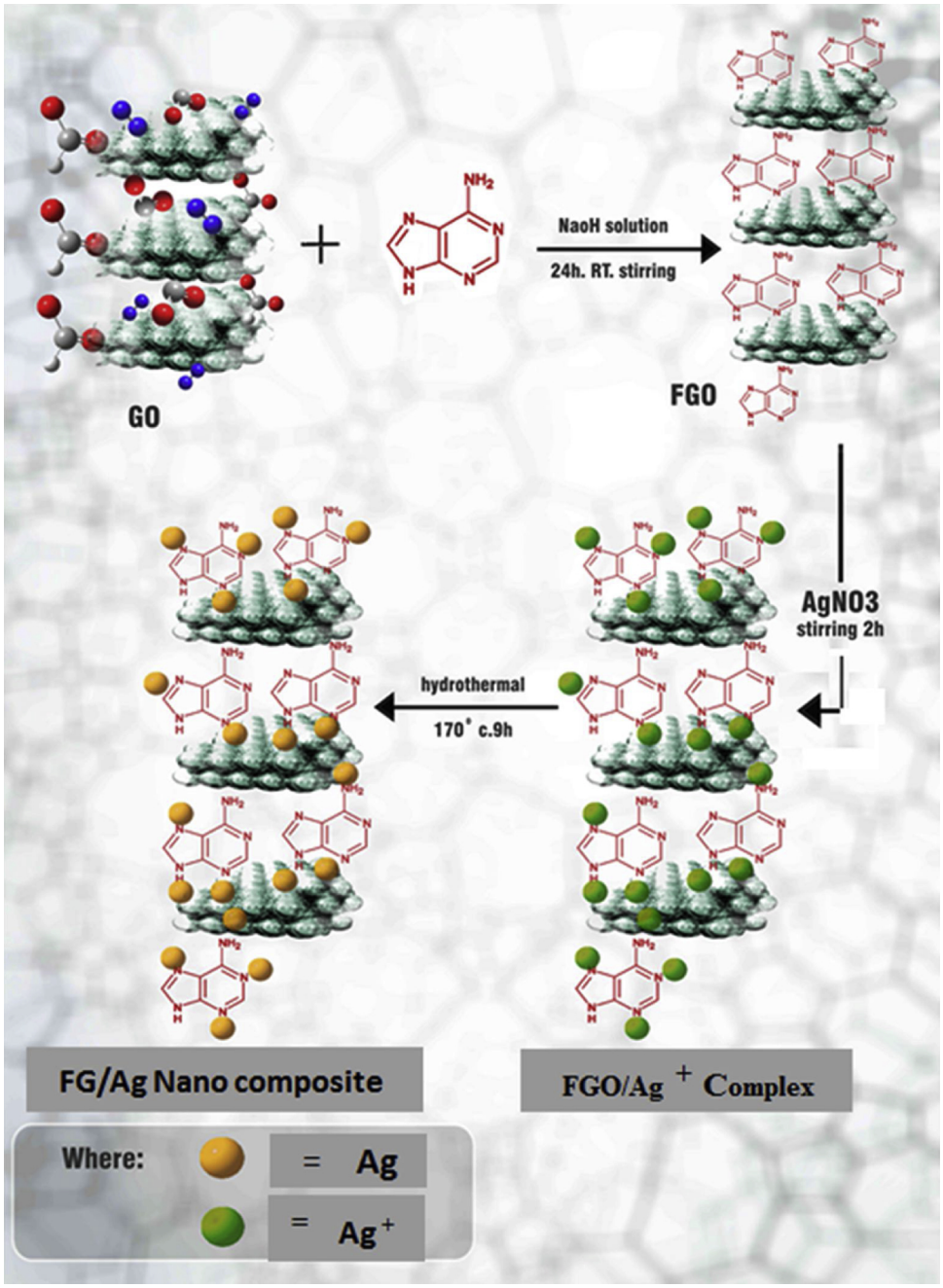

Fig. 1. Synthesis of FG/Ag nanocomposites via hydrothermal reduction.

2. Experimental methods and materials

2.1. Materials and chemicals

Graphite powder (< 20 μm), Nafion 117 solution (5%) and silver nitrate ($AgNO_3$) were purchased from Sigma Aldrich. Sulfuric acid (H_2SO_4, 99%) from Sham Lab., hydrogen peroxide (H_2O_2, 30% W/V) from LOBA Chemie, absolute ethanol and HCl (33%) were purchased from El-Nasr Pharmaceutical Company, Egypt. Finally, potassium permanganate ($KMnO_4$, 99%), from Arabic Laboratory Equipment Co., and Adenine (Merck) were used directly without further purification. Distillated water was used for washing the products.

2.2. Synthesis of spongy graphene oxide (SGO)

Graphene oxide (GO) was prepared from natural graphite using a modified Hummers' method [22]. In a typical experiment, graphite (1.5 g), $NaNO_3$ (1.5 g) and H_2SO_4 (70 ml) were mixed and stirred in an ice bath. Subsequently, 9 g of $KMnO_4$ were added slowly. The reaction mixture was warmed to 40 °C and stirred for 1 h. Water (100 ml) was then added and the temperature was increased to 90 °C for 30 min. Finally, 300 ml of water was added slowly followed by the slow addition of 10 ml of 30% H_2O_2. The reaction mixture was filtered and washed with 0.1 M HCl and water. The GO precipitate was dispersed in a water/methanol (1:5) mixture and purified with three repeated centrifugation steps at 10,000 rpm for 30 min. The purified sample was dispersed in deionized water and centrifuged at 2500 rpm and finally washed with deionized water and sonicated for 1 h to obtain highly exfoliated graphene oxide. The GO precipitate was dispersed in water/methanol mixture and purified with repeated centrifugation steps at 10,000 rpm for 30 min. Note that washing with 0.1 M HCl and water resulted in highly exfoliated GO sheets. To prepare spongy graphene

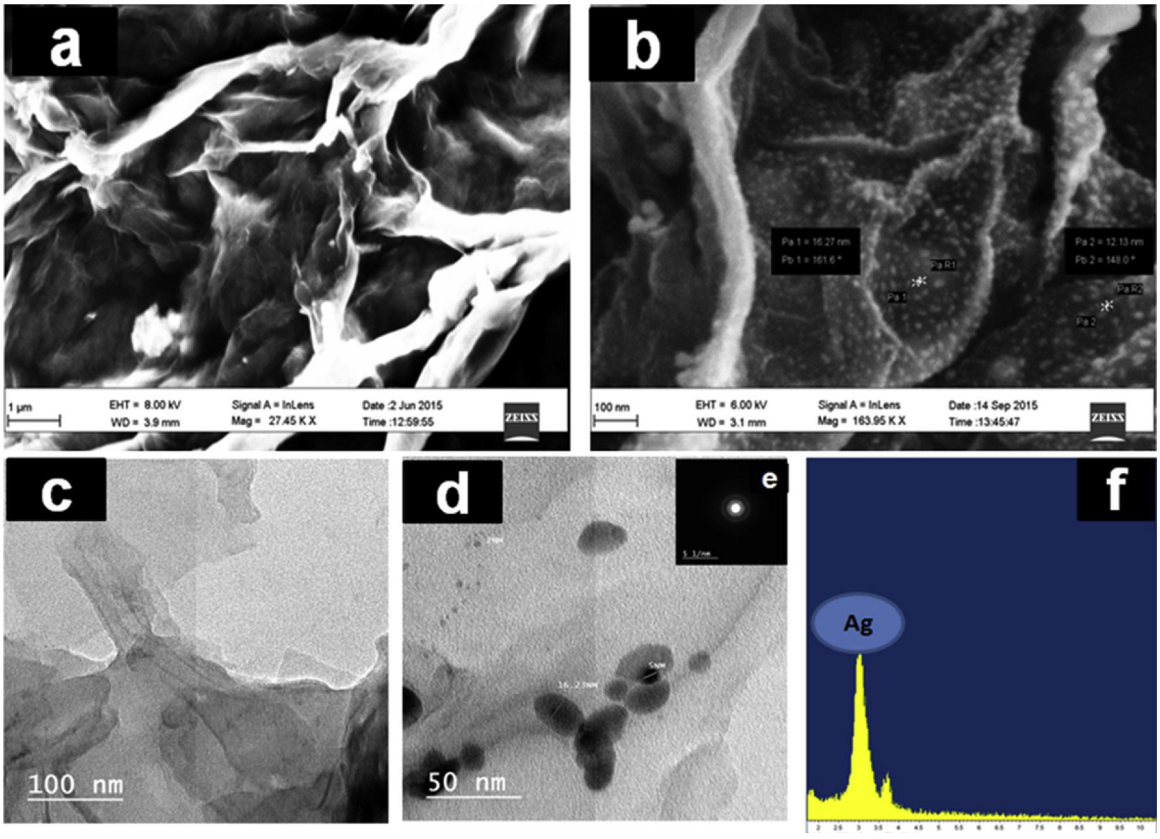

Fig. 2. FESEM Images of (a) spongy GO, (b) FG/Ag, the corresponding TEM images of (c) spongy GO, (d) FG/Ag, (e) the selected area electron diffraction pattern and (f) EDX spectra of FG/Ag nanoparticle.

oxide (SGO), GO solution (4 mg/l) was frozen at -18 °C for 2 days. After the GO solution was completely frozen, the tube was peregrinated to a freeze-dryer and dried at a temperature of -53 °C and a pressure of 10 Pa for 3 days [23].

2.3. Preparation of adenine-functionalized graphene oxide

GO (0.1 g) was dispersed in distilled water (10 ml), then (0.3 g) adenine and equimolar amount of NaOH in distilled water (10 ml) were added. The mixture was stirred for 24 h. The resulted precipitate was centrifuged, washed well with water/ethanol mixture and finally dried at 60 °C [24].

2.4. Preparation of functionalized graphene (FG-Ag Nano particles)

The functionalized graphene/silver nanoparticles (FG/Ag) composites were prepared by the hydrothermal reduction method. Typically a specific amount of FGO with silver nitrate equivalent to 10, 15 and 25 wt.% from FGO mass was added to 100 ml of deionized water, then the slurries were sonicated for 1 h to obtain a homogeneous dispersion and stirred at room temperature for 2 h to form FGO/Ag ion complex. The solution was transferred to a Teflon-lined autoclave and heated at 170 C^{o} for 8 h, and then allowed to cool to room temperature. The obtained black product was washed several times with deionized water and collected by centrifugation. Finally, the obtained FG/Ag nanocomposites were dried in oven at 60C; the samples are named as FG/Ag1, FG/Ag2 and FG/Ag3 for the 10, 15 and 25 wt.% $AgNO_3$, respectively.

2.5. Characterization techniques

The crystal structure of the prepared materials was examined by X-ray diffraction (XRD, XPERT- PRO- Analytical) with Cu Kα radiation (λ = 1.54°A). The surface morphology was investigated by field-emission scanning electron microscope (FESEM-Zeiss SEM Ultra-60) and high-resolution transmission electron microscope (HRTEM, JOEL JEM-2100) operating at an accelerating voltage of 120 kV. The infrared (IR) spectra were recorded using a JASCO spectrometer (FT/IR-6300 type A) in the range 400–4000 cm^{-1}. UV/Vis spectrophotometric measurements were made using a Shimadzu 2040 spectrophotometer. Raman measurements were performed using a micro-Raman microscope with an excitation laser beam wavelength of 325 nm. The weight loss of the samples was collected by TGA thermal analyzer (TA TGA-Q500) from room temperature to 800 °C at a heating rate of 10 °C/min in nitrogen atmosphere.

2.6. Preparation of electrodes and electrochemical measurements

All electrochemical measurements were done in a three-electrode system where the working electrode was made of a glassy carbon disk, the standard calomel electrode (SCE) and platinum wire were used as reference and counter electrodes, respectively. The electrochemical measurements were carried out in 0.5 M H2SO4 using Auto lab-302N electrochemical workstation (Metrohm). The cyclic voltammetry (CV) measurements were done in the potential range −0.2 to 1 V at various scan rates (1–200 mV/s). Galvanostatic charge/discharge measurements were done from −0.2 to 1 V at current densities of 0.4, 0.9, 1, 2, 3 A/g. The EIS measurements were performed at the open circuit potential over the frequency range of 0.01HZ to 100KHZ.

2.7. Assembly of FG-Ag2-based symmetric supercapacitor

The FG-Ag2 slurry was prepared by mixing 90% FG-Ag2 and 10 wt.% PVDF in DMF as a solvent, which was then drop-casted on graphite

sheet, followed by drying at 60 °C for 12 h. The assembly of the FG-Ag2//FG-Ag2 symmetric supercapacitors was performed by using FG-Ag2 as the negative and positive electrodes with a filter paper as the separator in 0.5 M H_2SO_4 solution as the electrolyte.

3. Results and discussion

Fig. 2 shows FESEM and TEM images of the fabricated materials. Fig. 2a depicts the surface of the fabricated spongy graphene oxide (SGO), revealing a large increase in the thickness of the layers, which is possibly due to the existence of oxygen groups in the basal plane of graphene. Upon functionalization with Adenine, Fig. 2b, the graphene (FG) becomes more exfoliated. Note also the uniformly distributed Ag-NPs on the graphene sheets upon hydrothermal treatment in $AgNO_3$. The average size of the Ag NPs is in the range 12–16 nm. Fig. 2c shows the corresponding TEM images, where the GO sheets appeared crumpled with lots of folds. The TEM image of the FG/Ag (Fig. 2d) shows a smooth and transparence surface and the appearance of silver NPs on the surface of graphene. Note that the morphology remained the same after the hydrothermal treatment. Fig. 2e shows the selected area electron diffraction (SAED) pattern of the FG/Ag nanocomposite with the ring-like diffraction pattern indicating the crystalline nature of the Ag NPs. The ring-like diffraction patterns can be assigned to the reflections from (111), (200), (220), and (311) lattice planes of face-centered cubic (FCC) Ag. Fig. 2f shows the EDX spectrum, confirming the presence of Ag NPs in the FG/Ag nanocomposite.

Fig. 3a shows the XRD pattern of pristine graphite, GO, FGO, FG and FG/Ag. The peak appeared in the diffraction pattern of graphite at 2θ = 26.5° corresponds to c-axis and reflection from the (0 0 2) plane with interlayer spacing of 0.34 nm. The spectra of graphite oxide (GO) showing a single and sharp diffraction peak at 2θ = 12°, corresponding to an interlayer spacing of 0.83 nm, confirm that GO is devoid of any graphite [25]. The rise in d-value of GO (from 0.34 to 0.83 nm) can be related to the increase of interlayer spacing along the c-axis, which can be attributed to the presence of oxygen atoms on the GO sheets [26]. The diffraction pattern of the adenine-functionalized GO exhibits both increasing and decreasing in the interlayer spacing. As a result of π-π stacking and hydrogen bond connections, the crystallinity of graphene is decreased and becomes somewhat amorphous. These factors enhanced the attraction between adjacent layers resulting in an irreversible aggregation or even restacking to graphite. Upon reducing the FGO via hydrothermal treatment, the sharp diffraction peaks at 2Θ of 24.7° and 12° disappeared, supporting the formation of graphene sheets (FG) and the complete reduction of GO. In the spectrum of FG/Ag, the major diffraction peaks at 38°, 44°, 61° and 77° can be assigned to the (1 1 1), (2 0 0), (2 2 0) and (3 1 1) planes of silver with a face-centered cubic (FCC) structure, respectively. The broad diffraction peaks of Ag indicate a relatively small crystallite size [27,28].

Fig. 3b shows the UV–vis absorption spectra of the synthesized materials. The GO electrode shows a strong peak centered at 231 nm with an extended shoulder at 300 nm, corresponding to π-π* transitions of aromatic C═C band and n-π* transitions of C═O band, respectively [28]. Upon functionalizing GO with Adenine to form FGO, the golden brown color of GO solution changed to dark brown for FGO because of the partial deoxygenation during functionalization. This results in a red-shift in the absorption peak to 246 nm, which can be related to the partial restoration of electronic conjugation in the aromatic carbon structure. The hydrothermal treatment results in simultaneous reduction of FGO to form FG. For FG/Ag, the 246 nm peak was further red-shifted to 264 nm, along with the appearance of a new peak at 410 nm

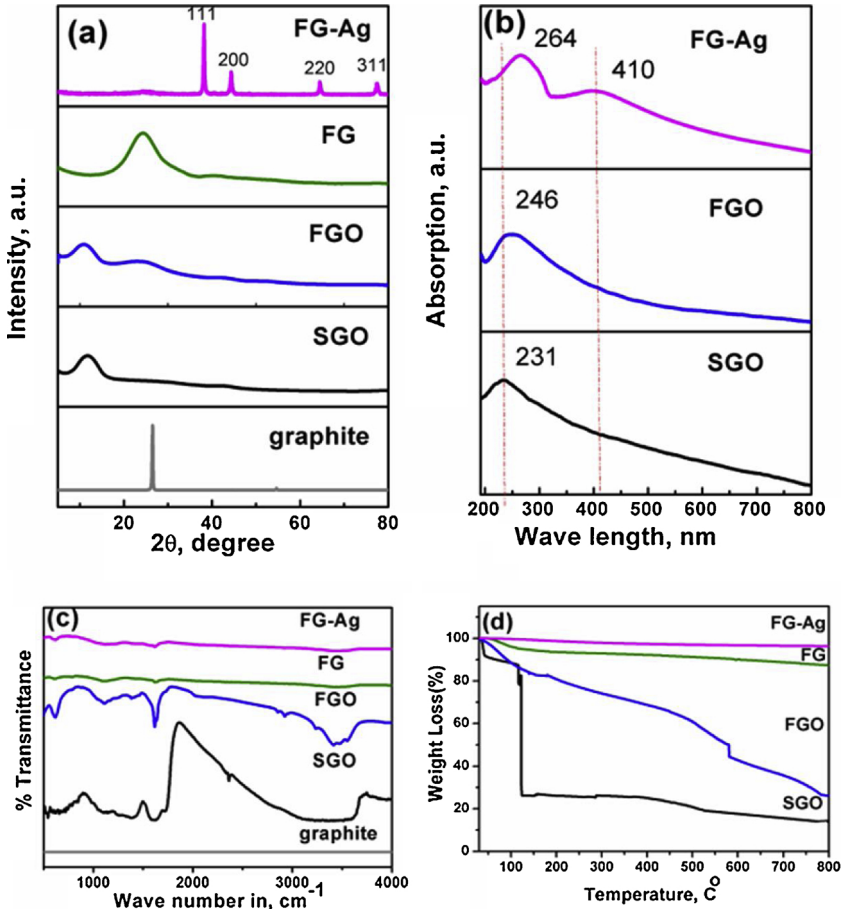

Fig. 3. (a) XRD pattern, (b) UV–vis absorption spectra, (c) FTIR spectra, and (d) TGA of the fabricated materials.

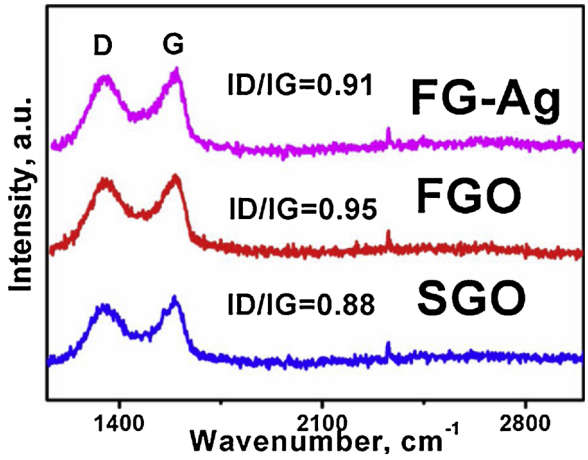

Fig. 4. Raman spectra of (a) GO, FGO and FG/Ag.

due to the excitation of surface plasmons of Ag NPs [28,29], confirming the formation of FG/Ag.

Fig. 3c shows the FTIR spectra of graphite, GO, FGO, FG and FG/Ag. Note that no functional groups were observed in the FTIR spectrum of graphite. However, many peaks for various functional groups were identified in the FTIR spectrum of GO. The broad band centered around 3563 cm^{-1} can be assigned to O—H stretching vibrations $\nu(OH_2)$, which can be attributed to adsorbed water. The other band appeared at 1725 cm^{-1} can be attributed to the stretching vibrations ν(C═O) of COOH group corresponding to carbonyl and carboxyl groups. The band at 1621 cm^{-1} attributed to in-plane vibration (C═C) from un-oxidized sp^2 CC bonds, the band at 1378 cm^{-1}corresponding to O—H deformation of C—OH group, and the band at 1101 cm^{-1} attributed to ν(C—O) stretching vibrations mode [30]. The peak at 1725 cm^{-1} almost disappears and a peak emerged at 1637 cm^{-1} specific of the C═O stretching in the amide group. Stretching of the amide C—N bond appears as a strong peak at 1188 cm^{-1}. The peaks at 1560 and 1618 cm^{-1} are attributed to the graphene vibration, and the peak attributed to the OH and NH stretching groups at 3475 cm^{-1} confirm the covalent functionalization of the neat graphite by adenine, assuring the successful functionalization process. The peak at 3415 $cm^{-1}$is specific for N—H stretching [31]. These results demonstrate that adenine molecules were covalently bonded to GO through the amide linkage. Note that the peak intensity of the C—O and C—O—C (epoxide) groups, respectively, decreased in FGO and after the hydrothermal reduction that resulted in FG. In contrast, the peak intensity of OH and carboxyl ions around 3000–3700 cm^{-1} was negligible in the FG/Ag nanocomposite, which can be attributed to the interaction between Ag NPs and carboxyl groups. Note also that the interaction between the Ag NPs and FG is very strong that they remained attached to the surface even after washing and strong sonication [32].

Fig. 3d shows the thermal stability of GO, FGO, FG and FG/Ag. The TGA analysis was carried out by heating the material under inert N_2 atmosphere to 800 °C at a rate of 10 °C/min. At temperatures below 100 °C, the mass loss can be associated with the elimination of adsorbed water. For GO, it is thermally unstable and losses weight in three steps; the first step is detected below 110 °C that can be related to vapor content and loss of interstitial H_2O [33] with a total mass loss of ~8%. The second stage is detected in the range 130–250 °C as a sharp drop peak that accounts for mass loss of~ 65%, which can be related to the decomposition of hydroxyl groups, introduced water on GO and carboxyl group to yield gases such as H_2O and CO_2. Note that CO_2 is usually produced due to the decomposition of carboxyl group because of thermal treatment at temperatures less than 500 °C. The third stage is extended from 350 °C up to 800 °C and the great mass loss became about 80%, which can be attributed to the decomposition of carbonyl group formed on the surface of graphene oxide to produce CO gas [34]. FGO showed higher thermal stability than GO. The first degradation step of FGO appeared almost at a similar range to that of GO (145–173 ∘C), whereas the second degradation step appeared at a much higher temperature of 365–415∘C. During the functionalization of GO with Adenine, the labile oxygen groups underwent chemical reaction to form a strong covalent bond with the amino groups of Adenine, which considerably decreased the amount of labile groups in FGO. Thus, very low weight loss was detected at around 145–173 °C in FGO. This result is also supported by the decrease in the FTIR peak intensity of the band at 1725 cm^{-1}, which is characteristic of the stretching vibrations ν(C═O) of COOH group corresponding to carbonyl and carboxyl groups that have disappeared, and the peak emergent at 1637 cm^{-1} is characteristic of the C═O stretching in the amide group [34], see Fig. 3b. The weight loss of the hydrothermally reduced FG shows a slight weight loss of about 10% up to 670 °C. These results show that the oxygen-based groups in GO formed heat-stable structures through covalent bonding with adenine. In the case of the FG/Ag nanocomposite, the weight loss of the sample was greatly limited. The reason is that the FG imposed a control on the mobilization of silver nanoparticles leading to homogeneous heating and prevention of heat concentration. This also supports a strong contact between FG and Ag NPs.

Raman spectroscopy is a powerful technique to investigate the structure and quality of carbon-based materials. Fig. 4 shows the Raman spectra for GO, FGO and FG/Ag. The intensity ratio of the D and G bands (I_D/I_G) is a suitable parameter for determining the sp^2 domain size of carbon structures containing $sp^3$and sp^2domains [35]. GO exhibited the G band at 1590.1 cm^{-1} and the D band at 1349.5 cm^{-1}. While the intensity of the D band for GO was enlarged compared to that of graphite, the G band is still prominent and the I_D/I_G ratio is 0.88. Upon functionalization of GO with Adenine, the G and D bands are shifted to 1593.6 and 1349.5 cm^{-1}, respectively and the D band becomes more prominent. The higher I_D/I_G ratio of FGO (0.95) than that of GO (0.88) indicates the introduction of sp^3 domain upon functionalization of GO with Adenine. However, the I_D/I_G ratio of FG/Ag is 0.91, slightly smaller than that of FGO (I_D/I_G = 0.95), indicating increased π-conjugation in aromatic carbons after the hydrothermal reduction. Therefore, the extensive oxidation and solvothermal reduction decreased the in-plane sp^2 domains and increased the edge planes, as well as the disorder in the prepared FG/Ag [35].

To study the supercapacitive performance of the fabricated samples, cyclic voltammetry (CV) measurements were performed in 0.5 M H_2SO_4, where the specific capacitance of the electrodes was calculated using Eq. 1.

$$Cs = \frac{\int Idv}{vm\Delta V} \quad (1)$$

where Cs is the specific capacitance, m is the weight of the electrode (g), I is the response current density (A/g), ΔV is the potential difference, and v is the potential scan rate (mV/s). Fig. 5a shows comparison of the cyclic voltammograms of FG/Ag1, FG/Ag2 and FG/Ag3 electrodes containing different Ag contents in the potential range of -0.2 to 1 V at a scan rate of 5 mV s^{-1}. The observed rectangular shape curves are characteristic of EDLCs. However, the observed redox peaks can be attributed to the presence of Ag NPs. It is also observed that the area under the CV loop of FG/Ag2 composite is larger than that of FG/Ag1, and FG/Ag3, indicating its higher capacitance. Note that increasing the amount of Ag NPs in the composite to 25 has resulted in decreasing the specific capacitance. This can be related to the presence of high concentration of Ag NPs that tend to agglomerate and block the pores of graphene, thus masking the effect of graphene nanosheets (GNS). The presence of GNS in the composite not only serves as highly conductive material but also provides high surface area that prevented the agglomeration of Ag NPs. Therefore, the Fg/Ag2 composition of graphene and Ag NPs has a maximum synergistic effect, thus resulting in the highest capacitive property. Fig. 5b. The specific capacitance of the FG/Ag2 electrode reached up to 567 F/g at a scan rate of 1 mV/s and drops

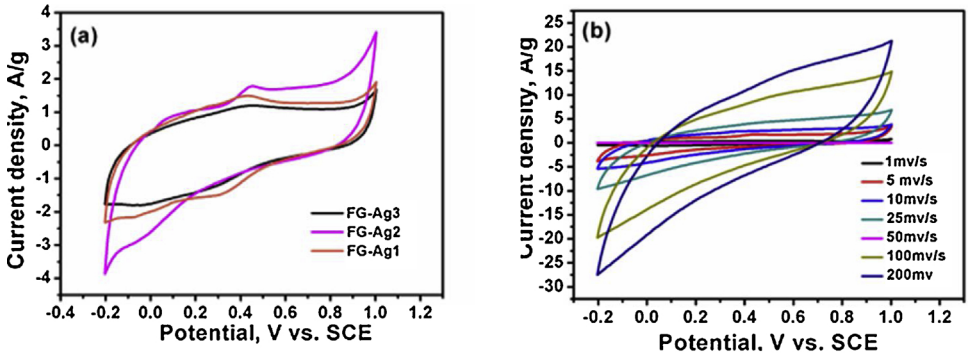

Fig. 5. (a) Comparative cyclic voltammograms of FG/Ag1, FG/Ag2, and FG/Ag3 nanocomposites at a scan rate of 5 mV/s, (b) cyclic voltammograms of FG/Ag2 electrodes at different scan rates c) comparative cyclic voltammograms of FG/Ag2, FG and SGO electrodes in 0.5 M H_2SO_4 at a scan rate of 5 mV/s, and (d) average specific capacitance of FG and FG/Ag2 electrodes at different scan rates in 0.5 M H_2SO_4.

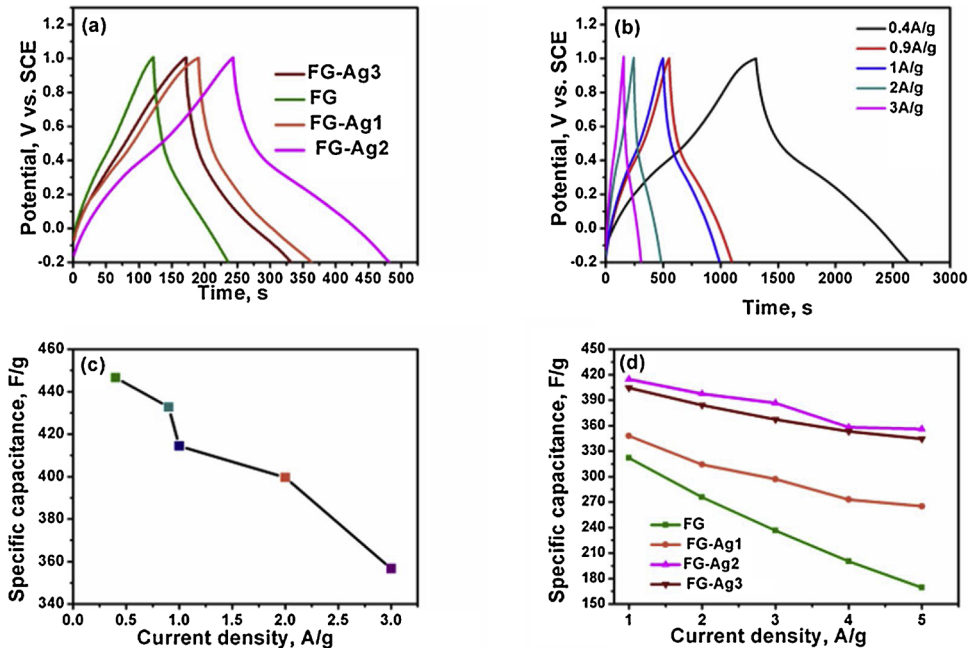

Fig. 6. (a) Comparative galvanostatic charge/discharge plots of FG, FG/Ag1, FG/Ag2, and FG/Ag3 nanocomposites at a constant charge/discharge current density of 2 A/g, (b) galvanostatic charge/discharge of FG/Ag2 at different current densities of 0.4, 0.9, 1, 2 and 3 A/g, (c) the corresponding specific capacitance of FG/Ag2 electrode at different current densities, and (d) average specific capacitance of FG, FG/Ag1, FG/Ag2, and FG/Ag3 at various current densities in 0.5 M H_2SO_4.

to 74.9 F/g at a scan rate of 200 mV/s, Fig. 5c shows the cyclic voltammograms of the FG/Ag, FG and SGO electrodes in 0.5 M H_2SO_4 at a scan rate of 5 mV/s. While the GO electrode showed insignificant current response due to its insulating properties, The FG electrode shows quasi-rectangular CV curve. The capacitance of the FG-Ag2 electrode is much higher than that of FG which can be related to the presence of silver nanoparticles and the presence of nitrogen atoms coming from adenine. The current of the FG-Ag2 electrode increases as the potential increases, suggesting an increasing electrical conductivity.

Irrespective of the scan rate, the FG/Ag electrode shows a weak cathodic (reduction) peak at ≈0.2VSCE and a corresponding anodic peak at ≈0.4 VSCE, Fig. 5d. This is a common phenomenon as the ions in the electrolyte might not have enough time to enter into the complex micropores of the electrodes (diffusion limited) at high scan speeds. Note that the obtained specific capacitance of 567 F/g at a scan rate of 1 mV/s is much higher than that previously reported for Ag–graphene nanocomposites prepared by hydrazine hydrate (220 F/g at a scan rate of 10 mV/s) [36], and silver-incorporated conductive polypyrrole (307.8 F/g at 2 mV/s) [37].

Galvanostatic charge/discharge measurements are essential to determine the performance of any material for use as a supercapacitor. Fig. 6a shows a comparison of the galvanostatic charge/discharge graphs for FG/Ag1, FG/Ag2 and FG/Ag3 electrodes in the potential range −0.2 to 1 V at a current density of 2 A/g. The FG/Ag2 nanocomposite achieved better specific capacitance (397.3 F/g at a 2 A/g) than FG/Ag1 and FG/Ag3 at the same current density. Fig. 6b shows the

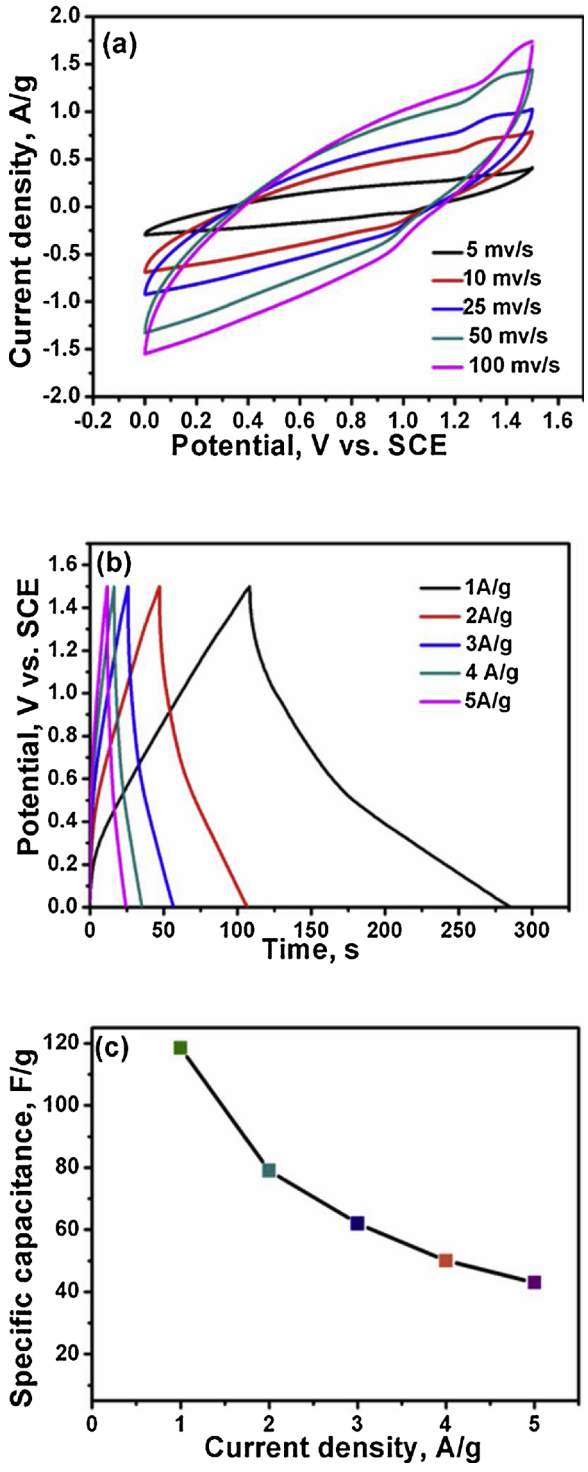

Fig. 7. (a) cyclic voltammograms of FG/Ag2 electrodes at different scan rates, (b) the corresponding specific capacitance of FG/Ag2 electrode at different current densities, and (c average specific capacitance of FG at various current densities in 0.5 M H_2SO_4 in a two-electrode system.

galvanostatic charge/discharge graphs for FG/Ag2 electrodes in the potential range −0.2 to 1 V at different current densities from 0.4 to 3 A/g. All the charge–discharge curves are quasi-triangular, indicating fast and capable charge transfer as well as high electrical conductivity [38]. This can be related to the existence of active nitrogen atoms from adenine with high electronegativity and the presence of Ag NPs that may generate dipoles on the surface of graphene [39,40], which attract charged species into the surface [41,42]. Fig. 6c shows the correlation between the specific capacitance and current density. Note that the specific capacitance of all samples decreases with the increasing the current density, Fig. 6d. The specific capacitance was calculated at different current densities using Eq. 2:

$$Cs = \frac{I\,\Delta t}{m\,\Delta V} \tag{2}$$

where I is the discharged current (A), Δt is the discharged time (s), and ΔV is the potential window (V). The calculated specific capacitance from charge/discharge curves of FG/Ag2 are 446.6, 432.7, 414.5, 397.3 and 386.7 F/g at 0.4, 0.9, 1, 2 and 3 A/g, respectively. The obtained specific capacitance at 0.4 A/g (446.6 F/g) is very close to that obtained from the CV curve (444 F/g), which is much higher than that previously reported for Ag NPs-decorated graphene (110 F/g at 0.5 A/g) [43]. Moreover, the FG/Ag2 electrodes exhibit excellent rate capability of 79.8% at a current density of 3A/g.

To evaluate the electrochemical performance of FG/Ag2, a symmetric two-electrode system (FG/Ag2// FG/Ag2) was fabricated with 0.5 M H_2SO_4 as the electrolyte. Fig. 7a shows the CV curves of the symmetric FG/Ag2 supercapacitor device at various scan rates. The GCD curves of the FG/Ag2 electrode at various current densities are illustrated in Figs. 7b and 8 c. The specific capacitances are found to be 118.5, 79, 62, 50 F, and 43 Fg^{-1} at current densities of 1, 2, 3, 4, and 5 A g^{-1}, respectively, see Table 1. Note that the presence of N heteroatom on the surface of functionalize graphene and silver nanoparticles enhances charge density and improves the redox reaction, generating high pseudocapacitance reflecting excellent charge/discharge reversibility of the FG/Ag2 material, which may be related to the enhanced electrical conductivity.

The energy and power densities are very important performance metrics of supercapacitors, which can be calculated from the galvanostatic charge/discharge graphs using Eqs.3 and 4.

$$E = \frac{1}{2}Cs(\Delta V)^2 = \frac{I\,\Delta V t}{2m} \tag{3}$$

$$P = \frac{E}{t} = \frac{I\,\Delta V}{m} \tag{4}$$

where E refers of the average energy density (Wh/Kg), P refers of average power density (W/Kg), Cs is the specific capacitance calculated from the charge/discharge curves, I is the discharge current (A), t is the discharge time (h), ΔV is the potential window (V), and m is the mass of the FG electrode (kg). Ragone's plot for the FG/Ag2 in three electrode and two electrode system at different current densities is shown in Fig. 7a. The energy density can reach up to 82.9 Wh/Kg with a power density of 600 W/kg at 1 A/g. Note that 71.34 Wh/Kg and 1800 W/Kg remains constant even at a current density as high as 3 A/g. It is worthy to mention that the achieved energy density for FG/Ag electrode (82.9 Wh/Kg at 1 A/g) is much higher than those reported for graphene (11.6 Wh/kg) [44], chemically-reduced graphene (11.5 Wh/Kg) [45], RGO (5.8 Wh/kg at 0.1 A/g) [46], graphitized composite of GO and onion-like carbon [47], and functionalized adenine-functionalized spongy graphene (64.42 Wh/Kg at 1 A/g) [16]. Fig. 8a shows that the assembled symmetric FG/Ag2 supercapacitor can deliver an energy density of 37.03 Wh kg^{-1} with a power density of 749.7 W/kg and retain 13.43 Wh kg^{-1} at 3750 W/kg, indicating rapid propagation of ions and electrons. A literature survey reveals that the energy density of FG/Ag2 supercapacitor is higher than those reported for graphene –based electrodes fabricated by different methods. [48–50], which can be related to the synergistic effect of adenine functionalization and Ag NPs decoration, see Table 2.

The cycle life test of the FG/Ag2 electrode was done by performing CV at a scan rate of 200 mV/s for 1000 cycles, Fig. 8b. The specific capacitance sharply increased from the initial cycle until 1000 cycle to reach 100.5% of the initial cycle, indicating the excellent cycling stability of the FG/Ag2 electrodes, which can be related to the increase of the electrolyte temperature during continuous operation over time.

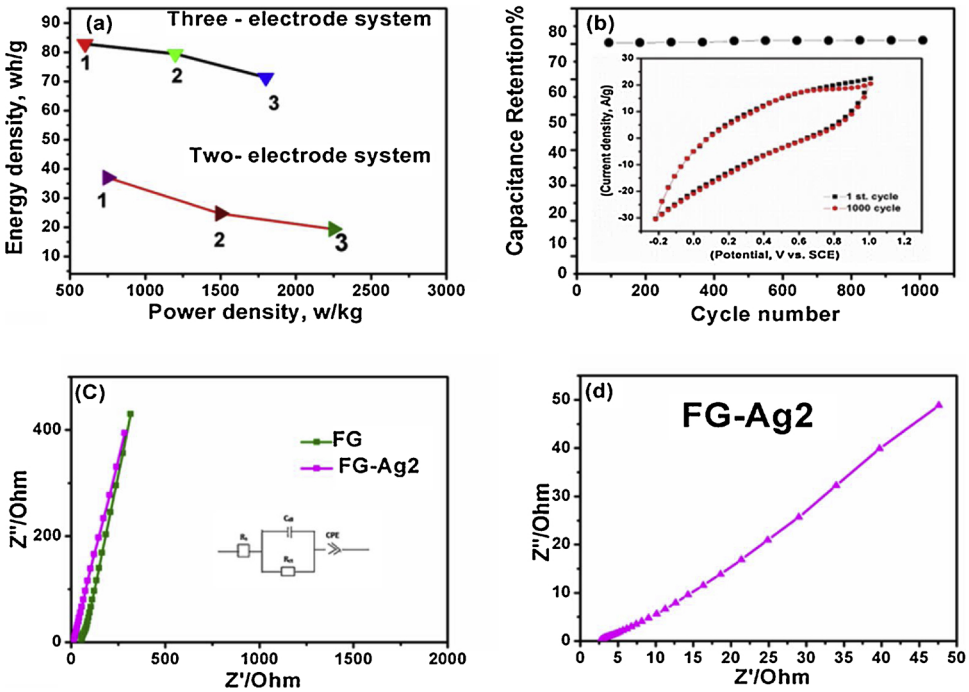

Fig. 8. (a) Comparative ragone plot for the FG/Ag2 electrodes in three-electrode system and two-electrode device at different current densities, (b) the first and 1000th CV cycles at a scan rate of 200 mV/s for the FG/Ag2 electrodes, (c) Nyquist plots of FG and FG-Ag2, and (d) Nyquist plot of FG-Ag2 in the two-electrode system device.

Table 1
The obtained specific capacitance for functionalized graphene with silver nanoparticles (FG-Ag2) in three-electrode and two-electrode systems.

Three – electrode system	**Specific capacitance (F/g) At differed scan rates**	**1 mV/s**	**5 mV/s**	**10 mV/s**	**25 mV/s**	**50 mV/s**	**100 mV/s**	**200 mV/s**
		567	444	342	218	161.4	130	81.4
	Specific capacitance (F/g) At different current densities	**0.4A/g**	**0.9A/g**	**1A/g**	**2A/g**	**3A/g**	**4A/g**	**5A/g**
		446.6	432.7	414.5	397.3	386.6	358	356

Two- electrode system	**Specific capacitance (F/g) At different current densities**	118.5	79	62	50	43
	energy density (Wh/Kg)	37.03	24.68	19.37	15.62	13.43
	power density (W/Kg)	749.7	1498.2	2250	2992	3750

Table 2
Comparison of the obtained specific capacitance to those reported in literature for doped graphene electrodes.

Material	Electrolyte	Specific capacitance (F/g)	Ref.
Ag–graphene nanocomposites	2 M KNO_3	220	[36]
Ag-incorporated conductive polypyrrole	1 M Na_2SO_4	307.8	[37]
Ag NPs-decorated graphene foam	2 M KOH	110	[43]
Sulfonated graphene/MnO_2/polyaniline	1 M Na_2SO_4	276	[48]
$CoFe_2O_4$/reduced graphene oxide/polyaniline	1 M KOH	257	[49]
Graphene/MnO_2/Polyaniline	0.5 M Na_2SO_4	380	[50]
Graphene–MnO_2–polyaniline	1 M H_2SO_4	395	[51]
Ag-decorated adenine-functionalized spongy graphene nanocomposites	0.5 M H_2SO_4	567	This work

The electrochemical impedance spectra of the synthesized FG and FG-Ag2 were measured in the frequency range of 0.1 Hz −106 Hz at open circuit potential with an amplitude of 5 mV. The Nyquist plots are shown in Fig. 8c composed of very small semicircle component at high-frequency followed by a linear component at low-frequency, indicating Faradaic charge storage mechanism. The small arc in the high-frequency region indicates low electronic resistance between graphene nanosheets [51]. The vertical line for an ideal electrode material, suggesting a good capacitive behavior of the fabricated electrode [46] with the equivalent circuit depicted in the inset of Fig. 8c. Note that Rs includes the electrolyte resistance and the active material/current collector contact resistance [51]. The obtained Rs values for FG, FG-Ag2 and FG-Ag2 in two-electrode were found to be about 54.06, 10.01, and 2.15 Ω, respectively. The absence of semicircle in the FG-Ag electrode reveals higher conductivity than FG due to the presence the silver nanoparticles [52].

4. Conclusions

Ag-decorated adenine functionalized spongy graphene (FG/Ag) nanocomposites were successfully synthesized via a simple and a green method. The electron microscopy (FESEM and TEM) analysis showed the homogenous distribution of the Ag nanoparticles (15–20 nm in size) on the surface of the functionalized graphene sheets. The FTIR analysis confirmed the covalent functionalization of the neat graphite with adenine, assuring the successful functionalization process, resulting in thermally stable materials as confirmed via the TGA analysis. Upon their use as supercapacitor electrodes, the FG/Ag2 nanocomposites showed a maximum specific capacitance of 567 F/g at a scan rate of 1 mV/s with excellent cycling retention of 100.5% after 1000 cycles at 200 mV/s. The energy density was 82.9 Wh/kg with a power density of 600 W/kg in the three electrode system and 37.03 Wh/kg with a power density of 749.7 W/kg at 1 A/g for the symmetric device. The observed

high performance, compared to those reported for bare graphene, can be related to the synergistic effects of the spongy structure, the adenine functionalization, and the decoration with Ag NPs.

Acknowledgements

The financial support of the present work by the National Research Centre and the American University in Cairo is highly appreciated.

References

[1] D.M. El-Gendy, N.A.A. Ghany, N.K. Allam, Green, single-pot synthesis of functionalized Na/N/P co-doped graphene nanosheets for high-performance supercapacitors, J. Electroanal. Chem. 837 (2019) 30–38.
[2] A.G. Pandolfo, A.F. Hollenkamp, Carbon properties and their role in supercapacitors, J. Power Sources 157 (2006) 11–27.
[3] M. Ramadan, A.M. Abdellah, S.G. Mohamed, N.K. Allam, 3D interconnected binder-free electrospun MnO@C nanofibers for supercapacitor devices, Sci. Rep. 8 (2018) 7988.
[4] A.E. Elkholy, F.E. Heakal, N.K. Allam, Nanostructured spinel manganese cobalt ferrite for high-performance supercapacitors, RSC Adv. 7 (2017) 51888–51895.
[5] A.E. Elkholy, F.E. Heakal, N.K. Allam, A facile electrosynthesis approach of amorphous Mn-Co-Fe ternary hydroxides as binder-free active electrode materials for high performance supercapacitors, Electrochim. Acta 296 (2019) 59–68.
[6] M.A. Mohamed, D.M. El-Gendy, N. Ahmed, C.E. Banks, N.K. Allam, 3D spongy graphene-modified screen-printed sensors for the voltammetric determination of the narcotic drug codeine, Biosens. Bioelectron. 101 (2018) 90–95.
[7] B.A. Ali, O.I. Metwalli, A.S.G. Khalil, N.K. Allam, Unveiling the effect of the structure of carbon material on the charge storage mechanism in MoS_2-based supercapacitors, ACS Omega 3 (2018) 16301–16308.
[8] N. Ahmed, B.A. Ali, M. Ramadan, N.K. Allam, Three-dimensional interconnected binder-free Mn-Ni-S nanosheets for high performance asymmetric supercapacitor devices with exceptional cyclic stability, ACS Appl. Energy Mater. (2019), https://doi.org/10.1021/acsaem.9b00435.
[9] S.G. Mohamed, S.Y. Attia, N.K. Allam, One-step, calcination-free synthesis of zinc cobaltite nanospheres for high-performance supercapacitors, Mater. Today Energy 4 (2017) 97–104.
[10] Y. Sun, Q. Wu, G. Shi, Graphene based new energy materials, Energy Environ. Sci. 4 (2011) 1113–1132.
[11] H.A. Ghaly, A.G. El-Deen, E.R. Souaya, N.K. Allam, Asymmetric supercapacitors based on 3D graphene-wrapped V_2O_5 nanospheres and Fe_3O_4@3D graphene electrodes with high power and energy densities, Electrochim. Acta 310 (2019) 58e69.
[12] J.R. Miller, R.A. Outlaw, B.C. Holloway, Graphene double-layer capacitor with ac line-filtering performance, Science 329 (2010) 1637–1639.
[13] W.S. Hummers, R.E. Offeman, Preparation of graphitic oxide, J. Am. Chem. Soc. 80 (1958) 1339.
[14] D.M. El-Gendy, I.M. Afifi, N.K. Allam, Eco-friendly, one-step synthesis of cobalt sulfide-decorated functionalized graphene for high-performance supercapacitors, J. Energy Storage 24 (2019) 100760.
[15] Y. Zhou, R. Ma, S.L. Candelaria, J. Wang, Q. Liu, E. Uchaker, P. Li, Y. Chen, G. Cao. Phosphorus/sulfur Co-doped porous carbon with enhanced specific capacitance for supercapacitor and improved catalytic activity for oxygen reduction reaction, J. Power Sources 314 (2016) 39e48.
[16] D.M. El-Gendy, N.A.A. Ghany, E.F. El Sherbini, N.K. Allam, Adenine-functionalized spongy graphene for green and high-performance supercapacitors, Sci. Rep. 7 (2017) 43104.
[17] Y.W. Zhu, S. Murali, W.W. Cai, X.S. Li, J.W. Suk, J.R. Potts, R.S. Ruoff, Graphene and graphene oxide: synthesis, properties, and applications, Adv. Mater. 22 (2010) 3906.
[18] L.-Q. Rong, C. Yang, Q.-Y. Qian, X.-H. Xia, Study of the nonenzymatic glucose sensor based on highly dispersed Pt nanoparticles supported on carbon nanotubes, Talanta 72 (2007) 819–824.
[19] W.B. Lu, F. Liao, Y.L. Luo, G.H. Chang, X.P. Sun, Hydrothermal synthesis of well-stable silver nanoparticles and their application for enzymeless hydrogen peroxide detection, Electrochim. Acta 56 (2011) 2295–2298.
[20] S. Liu, J.Q. Tian, L. Wang, X.P. Sun, A method for the production of reduced graphene oxide using benzylamine as a reducing and stabilizing agent and its subsequent decoration with Ag nanoparticles for enzymeless hydrogen peroxide detection, Carbon 49 (2011) 3158–3164.
[21] S. Park, R.S. Ruof, Chemical methods for the production of graphenes, Nat. Nontechnol. 4 (2009) 217–224.
[22] X. Xu, L. Pan, Y. Liu, T. Lu, Z. Sun, D.H.C. Chua, Facile synthesis of novel graphene sponge for high performance capacitive deionization, Sci. Rep. 5 (2015) 8458.
[23] S. Mallakpour, A. Abdolmaleki, S. Borandeh, Covalently functionalized graphene sheets with bio compatible natural amino acids, Appl. Surf. Sci. 307 (2014) 533–542.
[24] Y. Xu, H. Bai, G. Lu, C. Li, G. Shi, Flexible graphene films via the filtration of water-soluble non covalent functionalized graphene sheets, J. Am. Chem. Soc. 130 (2008) 5856.
[25] O.C. Compton, S.T. Nguyen, Graphene oxide, highly reduced graphene oxide, and Graphene: versatile building blocks for carbon-based materials, Small 6 (2010) 711–723.
[26] P. Guo, H. Song, X. Chen, X. Chen, Electrochemical performance of graphene nanosheets as anode material for lithium-ion batteries, Electrochem. Commun. 11 (2009) 1320–1324.
[27] C. Xu, X. Wang, Fabrication of flexible metal-nanoparticle films using graphene oxide sheets as substrates, Small 5 (2009) 2212–2217.
[28] J. Shen, M. Shi, N. Li, B. Yan, H. Ma, Y. Hu, M. Ya, Facile synthesis and application of Ag-chemically converted graphene nanocomposite, Nano Res. 3 (2010) 339–349.
[29] Y. Xu, Z. Liu, X. Zhang, Y. Wang, J. Tian, Y. Huang, Y. Ma, X. Zhang, Y. Chen, A graphene hybrid material covalently functionalized with porphyrin: synthesis and optical limiting property, Adv. Mater. 21 (2009) 1275–1279.
[30] D.M. El-Gendy, N.A. Abdel Ghany, N.K. Allam, Black titania nanotubes/spongy graphene nanocomposites for high-performance supercapacitors, RSC Adv. 9 (2019) 12555.
[31] R.V. Hull, L. Li, Y. Xing, C.C. Chusuei, Pt nanoparticle binding on functionalized multiwalled carbon nanotubes, Chem. Mater. 18 (2006) 1780–1788.
[32] C.D. Zangmeister, Preparation and evaluation of graphite oxide reduced at 220 °C, Chem. Mater. 22 (2010) 5625.
[33] Z. Lei, L. Lu, X.S. Zhao, The electrocapacitive properties of graphene oxide reduced by urea, Energy Environ. Sci. 5 (2012) 6391.
[34] H. Yang, F. Li, C. Shan, D. Han, Q. Zhang, L. Niu, A. Ivaska, Covalent functionalization of chemically converted graphene sheets via silane and its reinforcement, J. Mater. Chem. 19 (2009) 4632–4638.
[35] A.C. Ferrari, J.C. Meyer, V. Scardaci, C. Casiraghi, M. Lazzeri, F. Mauri, S. Piscanec, D. Jiang, K.S. Novoselov, S. Roth, A.K. Geim, Raman spectrum of graphene and graphene layers, Phys. Rev. Lett. 97 (2006) 187401.
[36] L. Zheng, G. Zhang, M. Zhang, S. Guo, Z.H. Liu, Preparation and capacitance performance of Ag–graphene based, J. Power Sources 201 (2012) 376–381.
[37] L. Yuan, C. Wan, X.Y. Fanhong, Facial synthesis of silver-incorporated conductive polypyrrole submicron spheres for supercapacitors, Electrochim. Acta 16 (2016) 31495.
[38] Z. WU, K. Parvez, A. Winter, H. Vieker, X. Liu, S. Han, A. Turchanin, X. Feng, K. Müllen, Layer-by-layer assembled hetero atom-doped graphene films with ultrahigh volumetric capacitance and rate capability for micro-supercapacitors, Adv. Mater. 26 (2014) 4552–4558.
[39] L. Sun, C. Tian, M. Li, X. Meng, L. Wang, R. Wang, J. Yina, H. Fu, From coconut shell to porous graphene-like nano sheets for high-power super- capacitors, J. Mater. Chem. A 1 (2013) 6462–6470.
[40] J. Hu, Z. Kang, F. Li, X. Huang, Graphene with three-dimensional architecture for high performance supercapacitor, Carbon 67 (2014) 221–229.
[41] H. Wang, T. Maiyalagan, X. Wang, Review on recent progress in nitrogen- doped graphene, synthesis, characterization, and its potential applications, ACS Catal. 2 (2012) 781–794.
[42] C.-M. Chen, Q. Zhang, X.-C. Zhao, B. Zhang, Q.-Q. Kong, M.-G. Yang, Q.-H. Yang, M.-Z. Wang, Y.-G. Yang, R. Schlöglb, D.S. Su, Hierarchically aminated graphene honey combs for electro- chemical capacitive energy storage, J. Mater. Chem. 22 (2012) 14076–14084.
[43] A. Bello, M. Fabiane, D. Dodoo-Arhin, K.I. Ozoemena, N. Manyala, Silver nanoparticles decorated on a three-dimensional graphene scaffold for electrochemical applications, J. Phys. Chem. Solids 75 (2014) 109–114.
[44] B. Abdul Hakeem, F. Mopeli, D.R. David, I.O. Kenneth, M. Ncholu, Silver nanoparticles decorated on a three-dimensional graphene scaffold for electrochemical applications, J. Phys. Chem. Solids 75 (2014) 109–114.
[45] S.-Y. Yang, K.-H. Chang, H.-W. Tien, Y.-F. Lee, S.-M. Li, Y.-S. Wang, J.-Y. Wang, C.-C.M. Ma, C.-C. Hu, Design and tailoring of a hierarchical graphene-carbon nanotube architecture for supercapacitors, J. Mater. Chem. 21 (2011) 2374.
[46] Z. Lei, N. Christova, X.S. Zhao, Intercalation of mesoporous carbon spheres between reduced graphene oxide sheets for preparing high-rate supercapacitor electrodes, Energy Environ. Sci. 4 (2011) 1866.
[47] M. Lianbo, S. Xiaoping, J. Zhenyuan, Z. Guoxing, Z. Hu, Ag nanoparticles decorated MnO_2/reduced graphene oxide as advanced electrode materials for supercapacitors, Chem. Eng. J. 252 (2014) 95–103.
[48] G. Feng, G. Shao, J. Qu, S. Lv, Y. Li, M. Wu, Tailoring of porous and nitrogen-rich carbons derived from hydrochar for high-performance supercapacitor electrodes, Electrochim. Acta 155 (2015) 201–208.
[49] Q. Xie, S. Zhou, A. Zheng, C. Xie, C. Yin, S. Wu, Y. Zhang, P. Zhao, Sandwich-lik nitrogen-enriched porous carbon/grapheme composites as electrodes for aqueous symmetric supercapacitors with high energy density, Electrochim. Acta 189 (2016) 22–31.
[50] K.V. Sankar, R.K. Selvan, Fabrication of flexible fiber supercapacitor using covalently grafted $CoFe_2O_4$/reduced graphene oxide/polyaniline and its electrochemical performances, Electrochim. Acta 213 (2016) 469–481.
[51] G. Yu, L. Hu, N. Liu, H. Wang, M. Vosgueritchian, Y. Yang, Enhancing the supercapacitor performance of graphene/MnO_2 nanostructured electrodes by conductive wrapping, Nano Lett. 11 (2011) 4438–4442.
[52] B. Mu, W. Zhang, S. Shao, A. Wang, Glycol-assisted synthesis of graphene-MnO_2-polyaniline ternary composites for high performance supercapacitor electrodes, Phys. Chem. Chem. Phys. 16 (2014) 7872–7880.